Article

Nondestructive Testing of High Reinforced Concrete Chimneys

Marek Maj [1,*], Andrzej Ubysz [2], Hala Hammadeh [3] and Farzat Askifi [4]

[1] Assistent Professor, Faculty of Civil Engineering, Wroclaw University of Science and Technology, Wroclaw, Poland; marek.maj@pwr.edu.pl
[2] Associate Professor, Faculty of Civil Engineering, Wroclaw University of Science and Technology, Wroclaw, Poland; andrzej.ubysz@pwr.edu.pl
[3] Associate Professor, Faculty of Engineering , Middle East University, Amman , Jordan; hhamm2131@gmail.com
[4] Assistant Professor, Department of Structure Engineering, Faculty of Civil Engineering, Damascus University, Damascus. Syria; frzat_askifi@hotmail.com
* Correspondence: marek.maj@pwr.edu.pl; Tel.: +48-601-729-184

Abstract: The nondestructive testing of reinforced concrete chimneys, especially the high ones, is an important element of the assessment of their condition, making it possible to forecast their safe service lifespan. Industrial chimneys are often exposed to the strong action of acidic substances – they are adversely affected by the flue gas condensate on the inside and by acid precipitation on the outside. Initially, this results in the corrosion of the shell concrete and then in the corrosion of the reinforcing steel. During the service life of such chimneys their condition should monitored in order to prevent structural failures and indicate the most endangered parts of the structure. Owing to thermographic surveys one can monitor the hazards leading to the degradation of the chimney structure, which is particularly vital when due to the character of the production process the chimney cannot be put out of operation. The methods for the interpretation of results from thermovision studies to determine the safety and durability of industrial chimneys are shown.

Keywords: nondestructive testing, thermographic surveys, monitoring of structures, reinforced concrete chimney, corrosion processes, service life of structure

1. Introduction

Industrial reinforced concrete chimneys often are often exposed to a chemically aggressive environment. The combustion gases conveyed via the chimney undergo condensation inside it or are dissolved in precipitation, becoming strongly acidic liquids. The concrete/acid contact results in the corrosion of the concrete and after the concrete cover is penetrated, also in the corrosion of the steel. The two corrosion processes result in the rapid degradation of the chimney structure.

As regards chimneys, one should bear in mind not only the high costs and the technological challenges involved in their construction, but also that they perform an essential role in the production processes and so cannot be put out of service for repairs. For example, in steel works and coking plants the damping of the furnace from which the combustion gases are conveyed to a chimney results in the destruction of the whole power unit. Therefore nondestructive tests are vital for both assessing the current technical condition of the chimney and monitoring the degradation processes over its whole service life [1].

2. Causes and effects of reduced effectiveness of chimney thermal insulation

One of the major causes of the degradation of the chimney's RC shell is the too rapid fall in the temperature of the combustion gas as it flows through the chimney flue. The chimney wall consists of the following three layers:

Peer-reviewed version available at Materials 2019, 12, 2027; doi:10.3390/ma12122027

- a reinforced concrete shaft,
- an internal wall (e.g. made of fire brick) constituting the chimney's inner lining which is very resistant to high temperatures,
- a mineral wool layer, placed between the two walls, serving as thermal insulation.

The durability of a chimney to a considerable degree depends on the quality and longevity of the thermal insulation. Since the chimney cannot be taken out of the production process, it is highly important to constantly monitor the condition of the insulation. Particularly suitable for this purpose are nondestructive testing methods. If the RC shell were removed in places to expose the insulation, the places could become corrosion centres and a thermal bridge could form.

When designing the geometry and thermal insulation of a chimney one should take into account the combustion gas inlet and outlet temperature, the amount and rate of flow of the flue gas and its condensation temperature. Significant internal forces can also arise from a temperature difference [2].

The above parameters are determined by:

- the amount of the exhausted gas,
- changes in flue gas temperature due to changes in the production technology,
- the daily changes of the physicochemical parameters of the chimney environment, such as the wind velocity, the atmospheric pressure, the air humidity, etc.

An important factor is the reduction in the insulating power of the chimney walls caused by changes in the physical properties of the insulation due to, e.g., the mineral wool getting damp [3]. As a result, the temperature of the flue gas in the chimney's upper part decreases and after the critical temperature is reached, this causes excessive flue gas condensation on the chimney lining.

Figure 1. Deposition of condensation on outer surface chimney wall along construction joints.

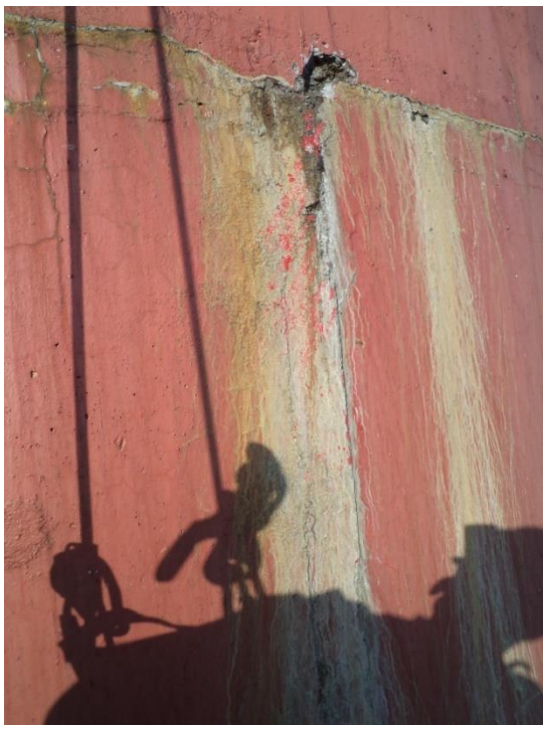

Figure 2. Condensation degrading of chimney wall.

As the condensate penetrates through cracks in the lining, it makes the mineral wool damp, whereby the latter loses its insulating properties. Moreover, the damp mineral wool sinks down and as a result, areas devoid of thermal insulation are created. As the coefficient of thermal conductivity decreases, the temperature of the chimney's inner wall falls further and so does the temperature of the flue gas. As a result, more and more flue gas condenses on the chimney's inner wall, whereby the degradation processes in the chimney's RC shell intensify (Figures 1, 2, 3).

Figure 3. Condensation dripping down from chimney upper ring

Figure 4. Condensation penetrating chimney crown wall

As condensation drips down the inner wall it penetrates via cracks to the mineral wool and outside to the reinforcement of the concrete wall, causing intense corrosion of the concrete and the reinforcing steel (fig. 4).

3. Idea of thermographic survey of chimney thermal insulation

Thermographic surveys have been used to detect thermal bridges in residential buildings for many years. Thermographic surveys are conducted using a camera which can take thermograms. In the case of chimneys, only external thermograms are taken. The air temperature considerably affects the accuracy of thermographic surveys. The latter are more precise, the larger the thermal contrast between the surface of the chimney shell and the ambient air temperature. Therefore the best period for evaluating the condition of the thermal insulation in chimneys is the winter season.

Passive thermography is the optimal method for the thermographic surveying of chimneys. On the basis of the thermographic images and reference readings one can determine the temperatures on the surface of the chimney shell [3, 4]. In this method the image is obtained for a set scale range. Knowing the temperature of the flow gas flowing through the chimney and the temperature on the outer surface of the chimney shell one can determine the actual thermal transmittance coefficient and compare it with its calculated values specified in the design documents. On the basis of the relative temperature differences one can determine the degree of damage to the thermal insulation.

4. Thermographic surveys of chimney thermal insulation

The monitoring of the condition of the chimney's insulation is an important element in the assessment of the durability of the chimney. On the basis of such monitoring one can forecast the actual service lifespan of the structure and systematically eliminate the causes of chimney shell degradation. The condition of the thermal insulation of industrial chimneys is examined using the classic thermographic method [5]. It is mainly the structure's envelope which is examined in this way to detect places where there are gaps in the insulation or there is no insulation. In the considered case, the thermograms showed that temperature differences on the chimney's outer surface occurred along practically its whole height and on its circumference (latitudinally). According to the results of the thermographic surveys of the 120 m high chimney with the lower and upper diameter of respectively D_d = 7.16 m and D_g = 4.48 m, the temperature difference in the particular points of the surface amounted to:

- as much as 21.8°C in the chimney's upper part,
- 15.9°C in the chimney's middle part,
- 10.5-11.9°C (being more uniform) in the chimney's lower part (Figure 5).

Peer-reviewed version available at Materials 2019, 12, 2027; doi:10.3390/ma12122027

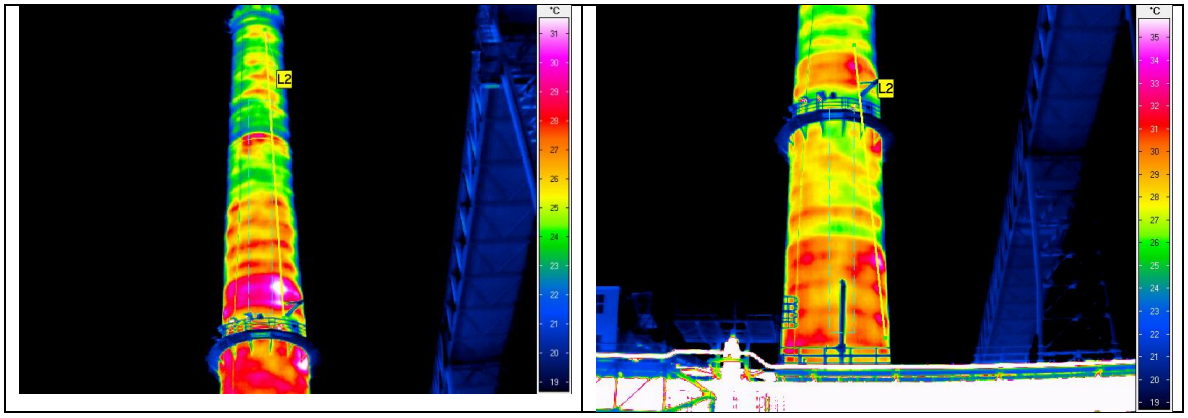

Figure 5. Chimney thermograms revealing insulation imperfections: (**a**) No thermal insulation more than two meters above and under platform; (**b**) Varied temperature distribution in chimney shaft.

The lower part of the chimney does not show such a high degree of degradation as its middle and upper parts. The thickness of the outer reinforced concrete shell, which is considerably greater in the lower part of the chimney, is one of the determining factors.

In order to nondestructively investigate the condition of the thermal insulation an analysis of temperature values ve on the outer surface of the chimney's shell was carried out. The parameters for the analysis had been determined on the basis of the known thermophysical characteristics of the materials, the chimney's geometry (specified in the design documents) and temperature measurements. The following parameters of the layered chimney wall were assumed for the analysis:

- thermal conductivity:
  - fire brick $\lambda = 1.30$ [W/(m K)],
  - mineral wool $\lambda = 0.05$ [W/(m K)],
  - reinforced concrete $\lambda = 1.74$ [W/(m K)],
- heat-insulating layer thickness:
  - fire brick layer – 11.4 cm,
  - mineral wool layer – 13 cm,
  - reinforced-concrete chimney shell wall – 24 cm,
- temperature:
  - inside chimney 200°C,
  - external 12.3°C.
- Temperature values ve on the outer surface of the chimney shell are:
  - for the wall with mineral wool: $v_e = 14.4$°C,
  - for the wall without mineral wall: $v_e = 32.4$°C.

Calculations and in-situ measurements indicate that in the places where the temperature of the reinforced-concrete shell is the highest there is no mineral wool or the wool there has very poor insulating properties. The measured minimum temperatures of the shell in well insulated places on average amounted to 17°C while the maximum temperatures in the same thermograms on average amounted to 33°C. The variation coefficient for the temperature on the chimney surface ranges from 0.13 to 0.25. The average decrease in thermal performance in the particular chimney wall surface areas ranges from 20% to 90%.

5. Thermal and static load analysis

As a result of the nonuniform temperature distribution, caused by damage to the thermal insulation, additional internal forces, such as bending moments, shear stresses and annular tensile and compressive forces, arise. The values of the forces can be traced by studying real cases of damaged chimneys.

5.1. Adopted assumptions

Peer-reviewed version available at Materials 2019, 12, 2027; doi:10.3390/ma12122027

The following were assumed: the velocity of flow of the flue gas in the chimney: v=10 m/s, the operating temperature of the flue gas at the chimney outlet: t_{w2}=180°C and the operating temperature of the flue gas at the chimney inlet: t_{w1}=220°C. The inlet of the combustion gas takes place through a connecting flue pipe located below the ground level.

The external design temperature was assumed on the basis of the national annex to standard [6, 7]: in winter T_{min}= -36°C and in summer T_{max}= +40°C.

Since no detailed information was available, the emergency flue gas temperature was assumed as 20 % higher than the typical one. The emergency temperature amounts to $t_{wa,1}$ =220°C and $t_{wa,2}$ = 270°C at respectively the chimney outlet and inlet. The emergency temperature was used in the calculations.

Researches of concrete were carried out with help of non-destructive and semi-destructive diagnostics of concrete structures. These methods are useful in assessment of construction durability [8, 9]. The conditions of foundation on piles were evaluated on the basis [10, 11].

5.2. Types of thermal effects in chimney

The first load results from the difference between the temperatures on the surface of the chimney shaft. The load was calculated for an ideal situation, i.e. immediately after chimney erection – no degraded insulation, and for a situation when some of the insulation has degraded. The temperature load was introduced as the gradient of the temperatures in the chimney shaft.

The second load stems from the difference between the chimney operating temperature during chimney service life and the initial temperature, i.e. the temperature at which the chimney was erected.

Distribution of temperature in chimney wall for undamaged insulation

The chimney wall consists of the following layers: the shaft, the thermal insulation and the lining. The thicknesses and diameters were assumed according to table 1. As the reference situation, the condition of the chimney immediately after its erection, i.e. with the continuous mineral wool and fibre brick insulation, was adopted. The following thermal conductivity coefficients were assumed: $\lambda_b = 1.74 W/mK$ for the reinforced concrete wall, $\lambda_{iz} = 0.05 W/mK$ for the insulation (mineral wool) and $\lambda_{sz} = 1.30\ W/mK$ for the fire brick.

Thermal transmittance coefficient k:

$$\frac{1}{k} = \frac{1}{\alpha_n} + \sum_i \left(\frac{t_i}{\lambda_i}\kappa_i \frac{r_z}{r_i}\right) + \frac{1}{\alpha_o}$$

where: $\alpha_n = 8 + v = 8 + 10 = 18 W/m^2K$ – the inflow coefficient (the zone of the inner surface of the lining), where v – the mean velocity of the flue gas;

$\alpha_o = 24 W/m^2K$ – the outflow coefficient (the outer surface of the shaft);

t_i – the thickness of layer i;

λ_i – the thermal conductivity coefficient of layer i;

r_i – the outside radius of layer i;

r_z – the outside radius of the shaft;

κ_i – correction coefficients taking into account wall curvature:

$$\kappa_i = \left(\frac{r_z}{r_i}\right)^{0.57}$$

where: $i = b$ for the reinforced concrete shaft, $i = iz$ for the mineral wool, $i = sz$ for the fire brick.

The temperature drop in a given layer is expressed by the formula:

$$\Delta T_i = k \frac{t_i}{\lambda_i}\kappa_i \frac{r_z}{r_i}\Delta t$$

where $\Delta t = t_w - t_z$

For the inflow and outflow the temperature drops are:

$$\Delta T_n = k \cdot \frac{1}{\alpha_n}\Delta t \qquad \Delta T_o = k \cdot \frac{1}{\alpha_o}\Delta t$$

Peer-reviewed version available at Materials 2019, 12, 2027; doi:10.3390/ma12122027

The temperature at the boundary of each of the layers is:

$$T_j = t_w - \frac{k}{\alpha_n} \cdot \Delta T - \sum_i \Delta T$$

Table 1. Geometric dimensions of thermographically surveyed existing chimney.

Segment no.	H	Shaft outside radius	Shaft outside diameter	Chimney wall thickness	Shaft inside radius	Shaft inside diameter	Insulation thickness	Lining thickness
-	[m]	[m]	[m]	[m]	[m]	[m]	[m]	[m]
1	2.5	4.00	8.00	0.42	3.58	7.16	0.15	0.23
2	15	3.80	7.61	0.39	3.41	6.83	0.15	0.23
3	30	3.61	7.21	0.36	3.25	6.49	0.13	0.23
4	45	3.41	6.82	0.33	3.08	6.16	0.13	0.114
5	60	3.21	6.42	0.3	2.91	5.82	0.13	0.114
6	75	3.01	6.03	0.27	2.74	5.49	0.13	0.114
7	90	2.82	5.63	0.24	2.58	5.15	0.13	0.114
8	105	2.62	5.24	0.21	2.41	4.82	0.13	0.114
9	120	2.42	4.84	0.18	2.24	4.48	0.13	0.114

Figures 6 and 7 show temperature drops in the particular layers in the winter season and in the summer season. The largest temperature drop occurs in the full insulation layer and it is about 10 times larger than in the reinforced concrete shaft. Because of the small thickness of the fire brick layer the temperature drop in this layer is the smallest.

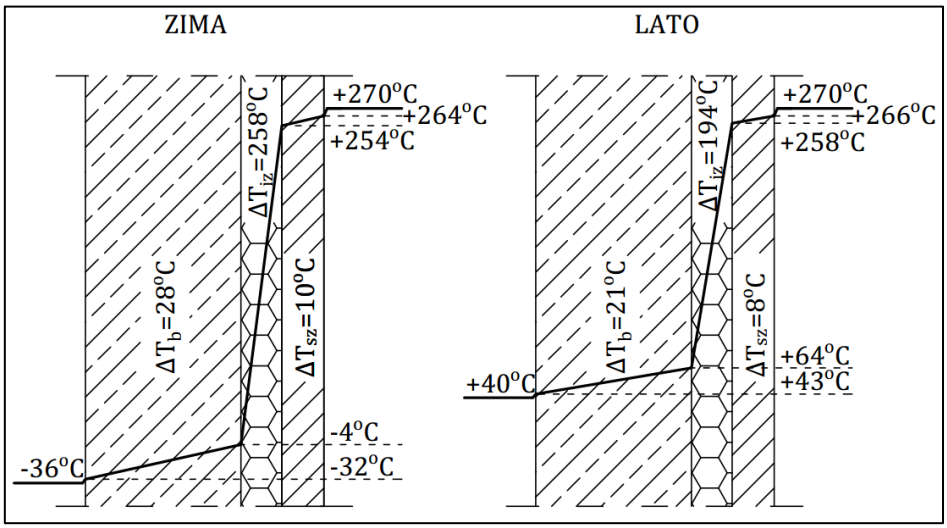

Figure 6. Temperature drops in particular layers for winter season and summer season.

Peer-reviewed version available at Materials 2019, 12, 2027; doi:10.3390/ma12122027

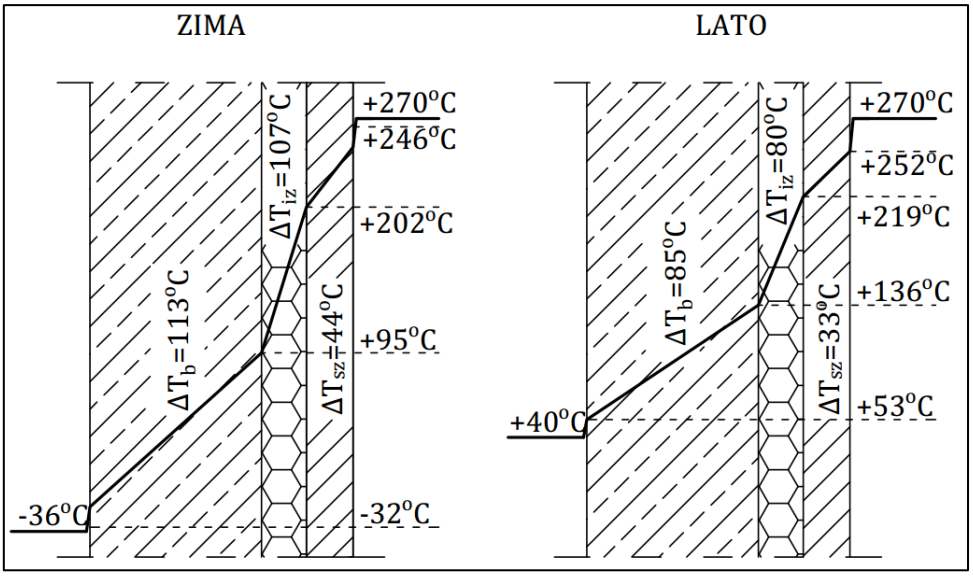

Figure 7. Temperature drops in particular layers of design chimney insulation in first segment with damaged insulation.

5.3. Distribution of temperature in chimney wall in case of insulation discontinuity

Insultation discontinuities were assumed to occur in 2.5 high segments uniformly distributed along the whole height of the chimney. The mineral wool in the segments was assumed to lack the design insulating power.

The temperature drops in the particular layers for the decreased mineral wool insulating power are shown in table 2. Since it is not possible to directly assess the degree to which the mineral wool's insulating power decreased, an approximate method was used. Calculations in which λ_{iz} was the unknown were carried out on the basis of the thermographic surveys of the existing chimney and the temperatures on its surface. The value of λ_{iz} was adjusted consistently with the actual temperatures on the surface of the investigated chimney. The results are presented in table. 3. The results apply to the 10-fold decrease in the insulating power of the mineral wool in the selected places ($\lambda_{iz} = 0.5W/mK$).

The maximum temperature gradient in the reinforced concrete shell in the winter season increased by about 420% in comparison with the gradient calculated for the worst insulation case. For the summer season temperature the gradient increased by about 405%. The temperature gradient which the insulation transfers is approximately equal to the gradient transferred by the chimney shaft under both the winter and summer temperature load. Such a large increase in temperature load can lead to the cracking of the reinforced concrete shell and to its damage. The temperature gradient values in the summer season and the temperature on the chimney's surface in summer and in winter and a figure showing the temperature gradient values in each of the layers are presented below.

In order to relate the assumptions to the actual temperature loading of the chimney the calculated gradients were compared with the temperatures appearing in the thermographic pictures of the existing chimney. The investigated real chimney is a 120 m high reinforced concrete structure serving a coke oven battery. The temperature of the combustion gas at the investigated chimney's inlet reaches 270°C (maximally 340°C) while the flue gas temperature at the outlet amounts to 220°C (maximally 300°C). The chimney is made of concrete C25/30 and reinforced with steel A-II. The chimney was divided into 9 segments, each about 15 m high. The chimney's insulation is made of semi-hard mineral wool boards and batts and its lining is made of fire brick. The thicknesses of the particular layers and their diameters are presented in table 1.

Peer-reviewed version available at Materials 2019, 12, 2027; doi:10.3390/ma12122027

Table 2. Temperatures on surface of calculated chimney at ambient temperature of 15°C.

Seg. no.	H		Tsz,w	Tsz,z	Tiz,z	Tb,z	Text.		Tsz,w	Tsz,z	Tiz,z	Tb,z	Text.
-	[m]		[°C]	[°C]	[°C]	[°C]	[°C]		[°C]	[°C]	[°C]	[°C]	[°C]
1	10	DAMAGED INSULATION	250	213	124	30	15	FULL INSULATION	265	256	41	19	15
2	20		246	208	118	30	15		261	252	39	19	15
3	30		241	203	112	30	15		257	248	38	19	15
4	40		234	192	118	32	15		251	240	42	20	15
5	50		230	187	111	33	15		247	236	40	20	15
6	60		223	175	113	35	15		241	227	44	21	15
7	70		218	169	106	35	15		237	223	41	21	15
8	80		212	160	103	37	15		232	216	42	22	15
9	90		207	153	95	37	15		228	212	39	22	15
10	100		204	150	94	37	15		224	208	38	21	15
11	110		200	148	92	36	15		220	204	38	21	15
12	120		193	142	89	35	15		212	197	37	21	15

The thermographic surveys revealed temperature differences on the chimney's surface, which indicates that the insulation was not uniform, there were gaps in it and in places the insulation had slid down and was damp. The temperature differences can also be due to the degradation of the reinforced concrete chimney shaft. Since the measurements were carried out outside the chimney the places with deteriorated thermal insulation are visible as dark red (the hottest places). The suspected places where the insulation is missing are visible in the thermograms as bands running at regular intervals around the circumference of the chimney. One can discern a certain pattern in insulation discontinuity: the bands are spaced at every 1-3 metres. The insulation loss is most visible in the lower part of the chimney and it is uniform there. In the thermographic picture the surface temperature in this part reaches about 34°C. In the segments situated higher one can see more distinct temperature differences on the outside surface, ranging from 22°C to 34°C.

Since the temperature of the flue gas in the existing chimney is comparable with the assumed emergency temperature in the chimney and also the diameters and thicknesses of the layers are similar, the temperature on the surface of the RC shaft, indicated by the thermographic surveys should be similar the one yielded by the calculations. As indicated by the high background temperature, the surveys were carried out in the summer season. The ambient temperature was assumed to be $15^{o}C$. The temperatures on the shaft surface calculated for the case with insulation and the case with insulation loss are comparable with the ones revealed by the thermographic surveys of the real chimney, as shown in the tables. For the assumed value of $\lambda_{iz} = 0.5W/mK$ the temperature on the RC shell is comparable with the temperature indicated by the thermographic surveys.

Temperature loading in 2.5 m high bands for alternately full insulation and damaged insulation was assumed. The values were assumed according to tables 2 and 3.

Peer-reviewed version available at Materials 2019, 12, 2027; doi:10.3390/ma12122027

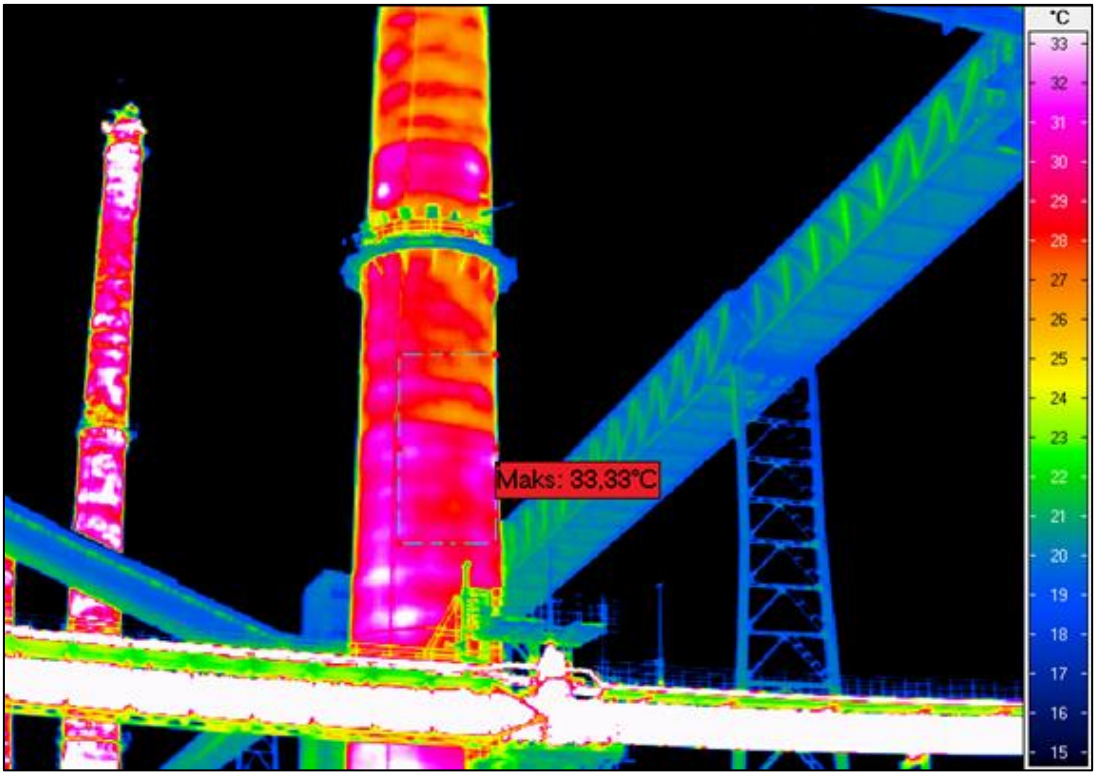

Figure 8. Thermographic picture of lower part of chimney shaft.

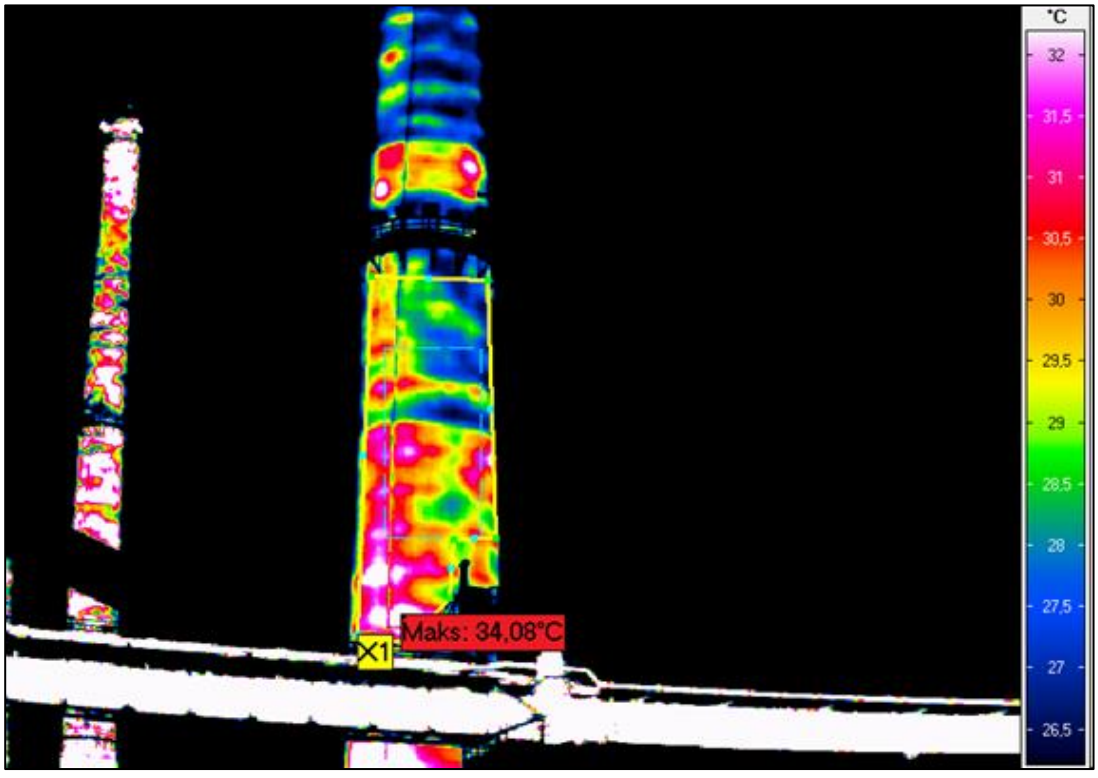

Figure 9. Thermographic picture of middle part of chimney shaft.

Peer-reviewed version available at *Materials* **2019**, *12*, 2027; doi:10.3390/ma12122027

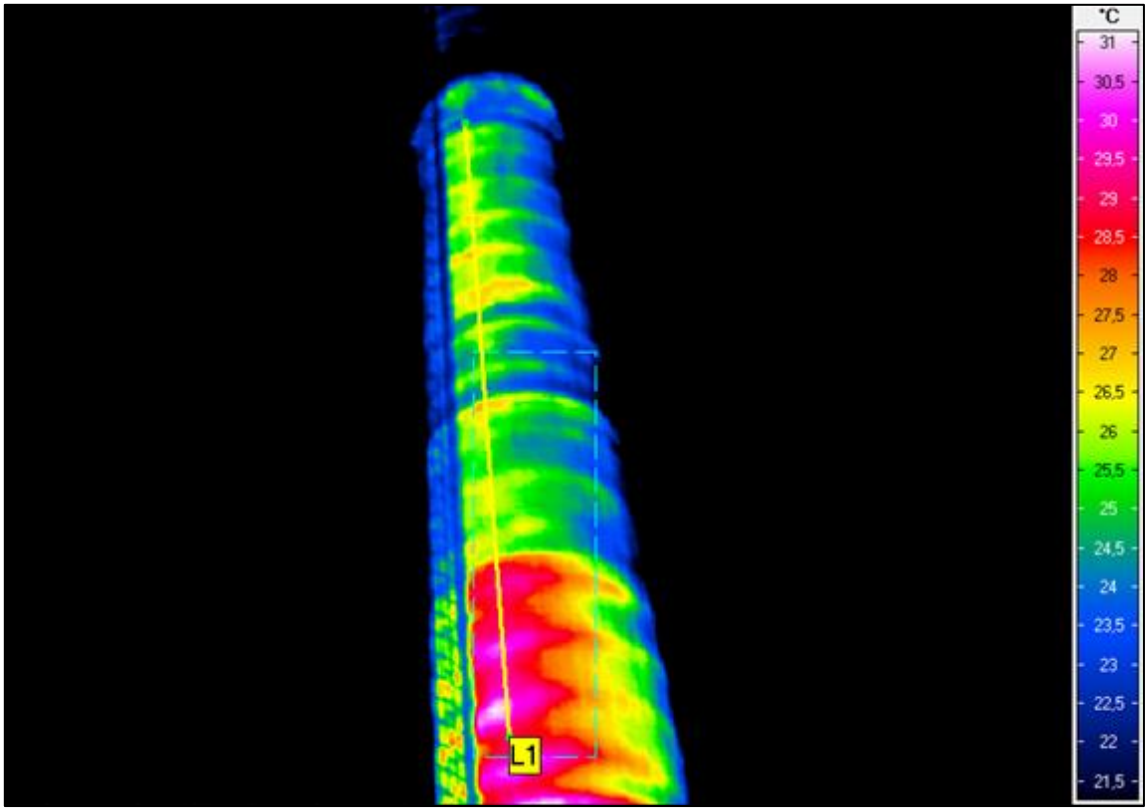

Figure 10. Thermographic picture of upper part of chimney shaft.

5.4. Surface temperature load

Since the chimney works at a temperature different than the one prevailing during its erection, a temperature load generating internal forces due to the chimney's limited freedom of deformation was assumed. Two load cases: the summer season load and the winter season load were considered. In each of the cases, a load at full insulation and a load at damaged insulation were analysed.

Table 3. Differences between chimney operating temperature and chimney erection temperature.

Seg. no.	H	WINTER		SUMMER	
-	[m]	INSULATION		INSULATION	
		FULL	DAMAGED	FULL	DAMAGED
1	10	-28	28	44	86
2	20	-29	25	43	83
3	30	-30	22	42	81
4	40	-27	27	44	84
5	50	-28	23	43	81
6	60	-25	26	45	83
7	70	-27	22	44	79
8	80	-25	21	45	79
9	90	-27	17	44	75
10	100	-28	16	43	74
11	110	-28	15	43	73
12	120	-29	13	42	71

The mean temperature in the wall can be calculated from the formula:

$$\bar{T} = T_{b,wew} - \frac{\Delta T_b}{2}$$

where $T_{b,wew}$ – the temperature on the inside surface of the reinforced concrete shaft; ΔT_b – the temperature drop in the reinforced concrete shaft.

The temperature at which the chimney had been erected was assumed as $T_o = 10^o C$.

The difference between the chimney operating temperature and the chimney erection temperature was calculated from the formula:

$$\Delta T = \bar{T} - T_o$$

5.5. Increase in bending moments due to increase in temperature gradient

The difference in the temperature distribution across the thickness of the reinforced concrete wall between the case with damage insulation and the case with undamaged insulation amounts to:

ΔT = 113 - 28 = 85 deg

Such big gradient causes additional bending moment and additional shear force.

The model of this calculations is presented on figure A1.

Calculations of this influence are included in the Appendix A

Additional thermally induced internal forces.

Let us consider the chimney as a cylindrical shell in which the unexpandable (well thermally insulated) band can be regarded as an element resembling a clamping tendon. Circumference L of the surrounding area with damaged thermal insulation is increased by ΔL due to higher temperature ΔT. The tendon with the introduced compressive force reduces the circumference to its size before the thermal expansion.

Using such a static load model one gets additional bending moment M and additional shear force Q (model is presented on figure B1. The calculation of these additional factors is presented in Appendix B

5. Conclusions emerging from investigations of thermal insulation of chimneys

The method of thermographic surveys, used to monitor thermal insulation in housing, also finds an important application in the investigation of the durability and failure hazard of industrial structures in which the condensation of chemically aggressive gases is likely to occur. This particularly applies to chimneys where invasive tests are not preferred because of the consequences of taking samples from the structure. Owing to thermographic surveys one can monitor the hazards leading to the degradation of the chimney structure. Flue gas condensate penetrates through cracks and leaks in the inner fire-brick lining into the insulation layer made of mineral wool. As a result, the insulation becomes damp and sinks down, whereby its insulating power decreases. This leads to intensified flue gas condensation and increased penetration of the condensate through leaks in the fire-brick wall into the layer of mineral wool, and also to increased condensation at the chimney crown level and consequently, to condensate dripping down on the outside surface of the reinforced concrete wall. The condensate penetrating through cracks in the RC shaft to the structural reinforcement intensifies the corrosion of the steel and the concrete. As a result of the decrease in insulating power the temperature in the shaft rises, whereby the bending moments and the tensile forces increase and the reinforced concrete shell cracks under the additional stresses which had not been taken into account in the design of the walls [2]. In the case of chimneys operating in the uninterruptable process mode, special measures are required to improve the condition of the insulation. The repair of the reinforced concrete chimney consisting solely in injection filling the external cracks [4] stops the corrosion of the reinforcing steel, but it does not improve the insulation of the chimney.

Author Contributions:

Conceptualization, Maj.M. and Ubysz.A.; Methodology, Maj.M.; Software, Hammadeh.H. and Askifi.F.; Validation, Maj.M., Ubysz.A., Hammadeh.H. and Askifi.F.; Formal Analysis, Maj.M. and Ubysz A.; Investigation, Maj.M. and Ubysz.A.; Resources, Maj.M., Ubysz.A., Hammadeh.H. and Askifi.F.; Data Curation,

Maj.M. and Ubysz.A.; Writing-Original Draft Preparation, Maj.M. and Ubysz.A.; Writing-Review & Editing, Maj.M., Ubysz.A., Hammadeh.H. and Askifi.F.; Visualization, Maj.M., Hammadeh.H. and Askifi.F.; Supervision, Ubysz.A;

Funding: This research received no external funding

Acknowledgments: Developed as part of the research project -" Industrialized construction process (Construction 4.0). Technological and methodological conditions of application of selected composite elements in civil engineering". This project is carried out by the Wroclaw University of Technology together with the Peoples' Friendship University of Russia in Moscow, Research Project PWr-RUDN 2017 no. 45WB/0001/17 Industrialized Construction Process.

Conflicts of Interest: The authors declare no conflict of interest.

Appendix A

$M_{\Delta t} = \alpha^* \Delta T * E_c J_c / t = 0{,}00001*85*33000000*1*0.242/12 = 134.5$ kNm

The cracking moment for the concrete

$M_{cr} = f_{ctm} W_1$ (1)

where: $E_c = 33$ GPa and $f_{ctm} = 2.9$ MPa – the mean tensile strength of the concrete (C30/37),

A_c – the cross-sectional area $A = 1*0.24 = 0.24$ m^2, $W_1 = bt^2/6$, b = 1 m, t = 0.24 m,

the bending section modulus for phase I.

$M_{cr} = 2.9*1*0.242/6 = 117$ kNm

Shear stress at damaged insulation/undamaged insulation boundary

The difference between the elongations of the adjacent rings depends on ΔT (for diameter $D = 6.68$ m):

$\Delta(\pi D) = \pi^* D^* \alpha^* \Delta T = 3.14*6.68*0.00001*85 = 20.98*0.00001*85 = 0.018$ m

The annular strain is

$\varepsilon = \Delta^*(\pi D) / (\pi^* D) = 0.018/20.98 = 0.000858.$

The annular force generated due to strain locking is:

$N = A_c * \varepsilon * E_c = 0{,}24*0{,}000858*33000000 = 6795{,}4$ kN/m

The force is blocked by horizontal surfaces with width t, whereby shear stress τ_c arises:

$\tau_c = N / (2*t) = 14.2$ MPa

at the mean shear strength of the concrete:

$f_{ctm} = 0.5 * f_{ctm} = 0.5*2.9 = 1.45$ MPa.

The above bending moments due to gradient ΔT, and shear forces are additional quantities, whereby the forces assumed in the design are exceeded.

Calculations were carried out for simplified static load diagrams. The values of the bending moments and shear stresses indicate high additional stresses in the concrete.

As the horizontal band in the concrete wall with damaged insulation heats up, the band is "pushed" outside more strongly, whereby a bending moment arises.

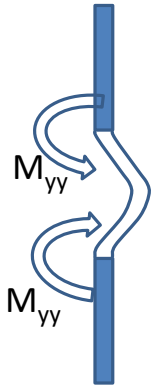

Figure A1. Change in length of cylindrical shell results in meridional bending moment.

As this displacement is blocked, annular force N=6795,4 kN/m is generated.

Appendix B

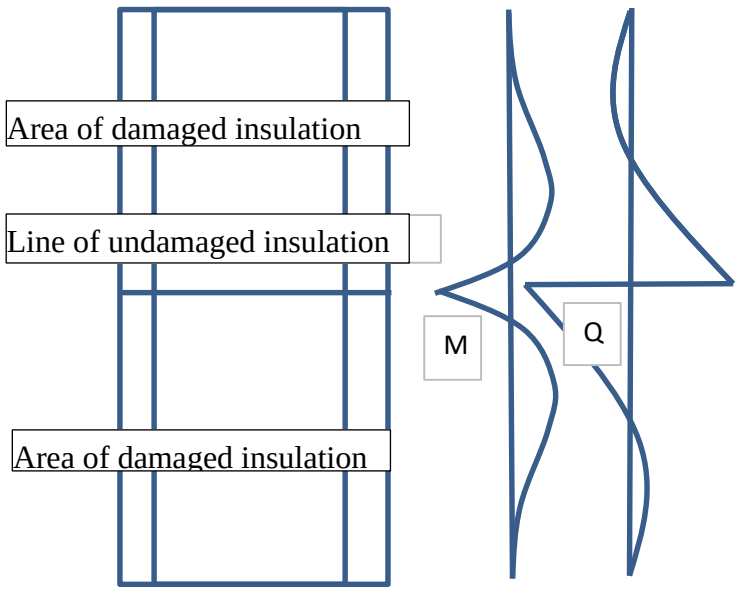

Figure B1. Model of influence damaged on undamaged area of insulation

In this case, calculations of the internal forces for design value ΔT obtained from the thermograms are as follows ([12]):

E_c=33 GPa

t - thickness=0.24 m

ν = 0.2

ΔT_{design} = 15 deg.

$D_{diameter}$ = 6.68 m

r =D/2 = 3.5 m

L= 20.986 m

ΔL = 0.003 m

N (force in shell, generated by ΔT) = 1188 kN/m

$\beta_p = [12*(1-\nu^2)/(D^2h^2)]^{(1/4)}*1.42$ ([12])

$\pi / (4\beta_p)$= 0.55 m

$F_{des} = N / r$ = 339.43 kN/m

$M = F_{des} / (4*\beta_p)$ = 59.70 kNm/m

$Q = F_{des} / 2$ = 169,71 kN/m

The above values added to the stress resulting from the permanent loads and the variable loads may contribute to horizontal cracking.

References

1. Dörr R., Noakowski P., Breddermann M., Leszinski .H, Potratz S. Verstärkung eines Stahlbetonschornsteins. *Beton- und Stahlbetonbau*, August **2004**, Vol.99(8), (pp.670-674).
2. Schnell J., Kautsch R., Noakowski P., Breddermann M. Verhalten von Hochbaudecken bei Zugkräften aus Zwang: Einfluß von Kriechen, Betonfestigkeit, Temperaturdifferenz, Plattendicke und Spannweite - Auswirkung auf Schnittgrößen, Stahlspannung, Rißbreite, Druckzonenhöhe und Durchbiegung. *Beton- und Stahlbetonbau*, 05/**2005**, Vol.100(5), (pp.406-415).

3. Jäger-Cañás A., Pasternak H. Influence of closely spaced ring-stiffeners on the axial buckling behavior of cylindrical shells. *ce/papers*, September **2017**, Vol.1(2-3), (pp.928-937).
4. Kaminski M., Maj M., Ubysz A., Chimney cracked reinforced concrete walls as a problem of durability exploitation, SEMC 2013: *The Fifth International Conference on Structural Engineering* 2-4.09.**2013**, Cape Town, South Africa.
5. Horváth L., Iványi M., Pasternak H., *Thermovision: an efficient tool for monitoring of steel members*. **1999**.
6. Świderski W. Metody i techniki termografii w podczerwieni w badaniach nieniszczących materiałów kompozytowych (Methods and techniques of infrared thermography in non-destructive testing of composite materials). *Problemy Techniki Uzbrojenia (Problems of Armament Technology)*. 1895-0973. R. 38, nr 4 (**2009**), (pp.75-92).
7. PN-EN 1991-1-5. *Oddziaływania na konstrukcje (Impact on structures)*, cz. 1-5: Oddziaływania termiczne (Thermal interactions). **2005**.
8. Hoła J., Bień J., Sadowski Ł., Schabowicz K., Non-destructive and semi-destructive diagnostics of concrete structures in assessment of their durability, *Bulletin of the Polish Academy of Sciences Technical Sciences*, **2015**, Vol. 63, 1, (pp. 87-96).
9. Gorzelańczyk T.; Hoła J.; Sadowski Ł.; Schabowicz K.: Methodology of nondestructive identification of defective concrete zones in unilaterally accessible massive members, *Journal of Civil Engineering and Management*, **2013**, Vol. 19, No. 6, (pp. 775-786).
10. Muszyński Z., Rybak J., Application for robust estimation methods for calculation of piles' ultimate resistance. *International Journal for Computational Civil and Structural Engineering*. **2013**, vol. 9, nr 3, (pp. 61-67).
11. Muszyński Z., Rybak J., Kaczor P., Accuracy assessment of semi-automatic measuring techniques applied to displacement control in self-balanced pile capacity testing appliance. Sensors (Basel) **2018**, vol. 18, nr 11, art. 4067, (pp. 1-23).
12. Timoshenko & Woinowsky S. *Theory of Plates and Shells (2nd Edition)*, McGraw-Hill Book Company, NY **1959**, (pp. 466-532).